An Approach of Adaptive Effective Cycles to Couple Fretting Wear and Creep in Finite-Element Modeling

Zupan Hu[a], Hai Wang[a], M. D. Thouless[a,b,*] and Wei Lu[a,*]

[a]*Department of Mechanical Engineering*

[b]*Department of Materials Science & Engineering*

University of Michigan

Ann Arbor, MI 48109, USA

(December 20, 2017)

[*] Corresponding author. Tel.: +1 734 647 7858; fax: +1 734 647 3170; E-mail addresses: thouless@umich.edu (M.D. Thouless), weilu@umich.edu (W. Lu)

Abstract

Fretting wear and creep can occur simultaneously when two surfaces in contact vibrate against each other at relatively high temperatures. An ability to analyze combined creep and wear is important for applications involving engines, contacting surfaces within fluids of high-temperature heat exchangers, such as fuel rods in nuclear power stations, and contact with polymers close to their glass-transition temperatures. The two phenomena of creep and wear interact with each other through their roles in affecting the shape and stress fields at contacts. Wear is a phenomenon that is generally considered to have no inherent time scale associated with it, beyond the period of the fretting oscillations. Traditional computational models for wear do not require a specific reference to time, but creep models do. Currently, a reliable and efficient numerical algorithm to couple the relatively long time scales of creep to the, generally, short periods of vibrations is not available. In this paper, we present such an algorithm, using an approach of adaptive effective vibration cycles. We demonstrate how to ensure the efficiency and reliability of the modeling by bounding the magnitude of the stress redistribution along the interface during the effective cycle. This approach enables the simulation of problems involving coupled wear and creep. We show that this approach is robust, and that it can be used during full-slip and partial-slip fretting for geometries with smooth or discontinuous interfaces at the edge of the contact. In particular, we use these examples to illustrate some of the crucial roles of creep in wear, such as transitions between partial and full slip.

Keywords: creep; fretting; wear modeling; finite element modeling; solid mechanics

1. Introduction

When an interface is subjected to oscillating loads at elevated temperatures, both wear and creep may occur. Both wear and creep can cause geometrical changes and stress relaxation that can affect the wear rate. This may affect the performance and lifetime of many structures such as biomechanics components (Bevill *et al.*, 2005; Jacobs *et al.*, 2002; Lee and Pienkowski, 1997; Teeter *et al.*, 2015), fuel rods in nuclear power stations (Kim *et al.*, 2008; Kim, 2010a; Lu *et al.*, 2016), thermal heat exchangers (Lai, 1979), and engine components (Gan *et al.*, 2017a; Narasimhan *et al.*, 1981; Takahashi *et al.*, 2002). While numerical models for the individual phenomena of wear or creep are fairly well established, algorithms to couple the two behaviors acting in concert have not been discussed in the literature.

The period of fretting vibration is usually much smaller than the time scale associated with the development of a significant amount of wear. In wear simulations, the wear depth is usually predicted using the Archard's law (Archard, 1953; Johnson, 1984), in which the local wear depth is proportional to the product of the local shear tractions and the local slip distance. Meaningful amounts of wear accumulate only over many cycles, since the wear in each loading cycle is very small. Therefore, it would be unnecessary and computationally expensive to update the contact geometry (or mesh) every cycle. Instead, the wear in one cycle is computed, and then multiplied by the number of cycles over which wear is assumed to be occurring without significant geometry changes so that the amount of wear in each subsequent cycle is the same. This algorithm is usually referred to as the Euler method (Gan *et al*., 2017b; Hegadekatte *et al.*, 2005; McColl *et al.*, 2004; Mukras *et al.*, 2009; Põdra and Andersson, 1999). The efficiency and reliability of the method depend on the choice of the number of cycles represented by one cycle, N. A value of N that is too large will cause excessive error because of stress redistribution, while

a value of N that is too small will reduce the efficiency. Therefore, a value of N that is reasonable at the beginning of the simulation can become inappropriate as wear propagates. An improved method is to determine the scale factor N dynamically so that the maximum wear increment is set to a threshold value (Põdra and Andersson, 1999). This method is reliable and efficient in simulations for which the worn interface is relatively smooth. However, in many engineering problems, the worn interface may not be smooth, and small local increments of wear may cause very large variations in the contact pressure. For example, in partial slip problems, very small increments of wear around the stick-slip boundary may result in very large changes of local contact pressure (Goryacheva *et al.*, 2001; Hu *et al.*, 2015). In these situations, using a wear-increment threshold may miss some dramatic changes of contact pressure, causing large errors in the predictions of wear. This suggests the need for an alternative criterion such as that presented in this paper as part of our desire to couple the effects of creep and wear.

It should be noted that the approach described above works because there is no inherent time scale associated with the wear model. Conversely, consideration of creep does bring in time scales associated with the creep mechanisms that may change as the stress or temperature changes. Constitutive laws associated with various creep mechanisms are used to describe the relationships between the strain rate and stress in different regimes of stress and temperature (Frost and Ashby, 1982; Wang et al., 2013), and can be incorporated in finite-element codes (Wang *et al*., 2013). When wear and creep act together, one cannot simply multiple the amount of wear in one cycle by the number of cycles to get the total effect, since creep happens continuously over time and is different between each cycle. There is no such concept that the creep in one cycle can represent the creep in subsequent cycles.

The fundamental problem in developing efficient algorithms for combined creep and wear is that creep has an inherent time scale associated with it, but is independent of sliding distance, while wear is independent of time except through the vibrational frequency, which does not enter directly into the analysis. Efficient algorithms for wear use criteria based on sliding distances or wear depth. Efficient algorithms for creep use criteria based on characteristic times for stress relaxation. Although one can convert the wear criteria to ones based on time through the vibrational frequency, the choice of a computational time increment based on either one of them may be inappropriate for the other, and cause excessive error. Therefore, one goal of this research was to determine an efficient algorithm to couple the time scales of vibration and creep, through their effects on wear. A second goal of this research was to explore how creep might affect wear. In this context it is noted that stress relaxation could have two competing effects: (i) reduction of normal pressure could enhance slip and, hence, the wear rate; (ii) reduction of normal pressure could reduce Coulomb friction and, hence, the associated frictional work and wear rate. Both of these effects will be observed in the results presented in this paper.

We consider stress redistribution along the contact surface to be the concept that connects creep and wear. For example, the stress redistribution caused by creep can affect the local contact pressure and, hence, the propensity to slip, which affects the wear rate. It should also be noted that, unless diffusional (linear) creep is the dominant creep mechanism, creep changes the singularity of the stress fields near the corners of contacts. This may affect the critical coefficient of friction for slip. Furthermore, in many engineering applications, preloaded components are designed to achieve full-stick conditions at the contact interface. However, creep can relax the contact pressure. In some circumstances, this can lower the shear tractions (through Coulomb's Law) resulting in lower wear rates. In other circumstances, this relaxation

can enable a zone of partial slip to spread across the interface until full slip occurs, perhaps increasing the wear rate. There are also problems in which wear occurs within a partial slip zone at a contact edge that cannot spread according to traditional wear analyses (Goryacheva et al., 2001; Hu et al., 2015), but may spread if the ratio of the normal and shear tractions are affected by non-linear deformation (Hu *et al.*, 2015). Finally, it should be noted that geometrical changes in the contact surface that result from wear may redistribute contact pressures, and affect the local creep rates.

In conclusion, creep and wear interact through stress redistribution along the contact surface. Therefore, the use of a criterion that limits the change in contact pressure to within a pre-defined threshold should be useful to couple creep and wear accurately and efficiently. This concept is developed in more detail within this paper.

2. Methodology

2.1 Coupling vibration, creep and wear by effective cycles

The period of fretting vibration is usually much smaller the time scale over which significant wear or creep occurs. For example, the period of vibration for grid-to-rod fretting in nuclear reactors is seconds or less (Kim, 2009, 2010b), while the time scale for significant stress redistribution associated with creep or wear can be months or years. This huge difference in time scales poses a significant challenge when attempting to couple their effects in a numerical simulation of this important problem.

According to Archard's law (Archard, 1953), the local increase in wear depth during any increment of time is proportional to the local frictional work done during that increment. With an assumption of Coulomb friction, the local frictional traction is given by the product of the

coefficient of friction and the local contact pressure. Therefore, at any time t and location, x, along a contacting surface, the increment of wear depth accumulated during a small increment of time δt is given by

$$\delta w(x,\delta t) = \alpha_o \mu p(x,t) \delta s(x,\delta t), \tag{1}$$

where α_o is the wear coefficient, μ is the coefficient of friction, $p(x, t)$ is the local contact pressure, and $\delta s(x, \delta t)$ is the local slip during the time increment. This equation is always valid, provided friction is governed by Coulomb's law. (In the trivial case where there is no slip, the equation is still valid, since $\delta s(x, \delta t) = 0$.) In the equation given above we have assumed that the contact pressure varies in only one dimension along an interface; obviously, the equation can be readily generalized to two dimensions.

Generally, Archard's law with a constant wear coefficient is applicable for full slip, when wear debris is continuously removed. With partial slip there is a possible issue in that wear debris may accumulate. In this context, it is noted that it has been shown experimentally that with debris accumulation, wear behavior can reach a steady state in which the Archard's law with a constant wear coefficient is also appropriate (Costa et al., 2017; Hong et al., 2017; Williams, 2005). In the transient state before a steady state is reached, a varying friction or wear coefficient would need to be used, so Archard's law would not be strictly appropriate. However, in the absence of published experimental data on how the wear coefficient might vary during partial slip when debris might not be ejected from the contact, we follow a simplifying assumption used by others in the field (Ding et al., 2004; Fouvry et al., 2001; Goryacheva et al., 2001; Johansson, 1994; Kasarekar et al., 2007; Oqvist, 2001; Põdra and Andersson, 1999; Rezaei et al., 2012), and assume a constant wear coefficient throughout the wear process.

To implement Archard's law with Coulomb friction in a finite-element model, it is necessary to monitor the distribution of the contact pressure for all the nodes along an interface at time t_i, and the corresponding slip distance for each of those nodes that accumulates during a computational-time increment δt_m. Equation (1) then gives the incremental increases in wear depth for each node during δt_m. These wear depths can then be integrated for all subsequent time steps and added to the wear distribution at time t_i, $w(x,t_i)$, to find the total wear depth at a time $t_i+\Delta t$:

$$w(x,t_i+\Delta t) = w(x,t_i) + \sum_{m=1}^{M} \alpha_o \mu p(x,t) \delta s_m(x,\delta t_m) . \tag{2}$$

Here M is the total number of computational increments to advance Δt, i.e. $\Delta t = \sum_{m=1}^{M} \delta t_m$.

An efficient algorithm is provided by analyzing two full cycles, and recognizing that the slip distances for any point x remain the same in the second and subsequent cycles, provided p remains unchanged between cycles, i.e. $p(x,t)= p(x,t+T_o)$, where T_o is the period of the physical oscillation. Therefore, the wear at any point after an arbitrary number of cycles, N, is approximately given by N times the wear in a single cycle. This is the basis of many numerical wear models. The limit to how many cycles can be represented by this approach depends on the extent to which geometry changes associated with wear affect the pressure distribution along the interface. Eventually, the geometry will need to be updated, and a new pressure distribution calculated.

If one chooses to think of the algorithm described above as resulting in an effective cycle, one should note that any consideration of the period of the effective cycle is irrelevant; effectively, it is the wear coefficient that is changed. This marks a point of departure from the

algorithm proposed in this paper, in which the period of the effective cycle needs to be considered when accounting for creep.

The creep laws and their corresponding time-scales depend on the relevant creep mechanism (Frost and Ashby, 1982; Wang et al., 2013). In this paper, we will use a simple power law of

$$\dot{\tilde{\varepsilon}} = A\tilde{\sigma}^n \tag{3}$$

where $\dot{\tilde{\varepsilon}}$ is the von Mises effective creep strain rate, $\tilde{\sigma}$ is von Mises effective stress, and A and n are constants depending on the temperature and microstructure[1]. We will not consider the effects of temperature or mechanism change in this paper, but note that the numerical approach we develop here can be used with multi-mechanism creep models (Wang *et al.*, 2013), as illustrated by a specific example related to wear in a nuclear-power plant (Wang *et al.*, 2017).

Linear isotropy is assumed to link the stress and strain tensors within the contacting bodies. During any increment of computational time, incremental changes in the strain tensor are computed using the Levy-Mises flow rule (Akhtar S. Khan and Huang, 1995) for creep, and modified stresses are re-calculated from the new strain tensor. These calculations allow the pressure distribution to be calculated as a function of time along the interface.

In order to compare the effects of creep and wear on the change in the contact pressure, it is necessary to introduce the concept of a time scale into the effective cycle. This is illustrated in Fig. 1. Not only does the wear coefficient have to be magnified so that the wear depth is calculated correctly in a single effective cycle, but the period must also be increased so that the stress relaxation is calculated correctly. If the period of the physical oscillations is T_o, and the

[1] Note that for an oscillating stress whose amplitude is considerably smaller than the mean, frequency has no effect on the accumulated creep strain.

period of the effective cycle is T_i, then the effective wear coefficient is $\alpha_o T_i/T_o$. The wear depth after one effective cycle T_i from time t_i is given by

$$w(x,t_i+T_i) = w(x,t_i) + \frac{\alpha_0 \mu T_i}{T_o} \sum_{m=1}^{M} p\left(x,t\right) \delta s_m(x,\delta t_m). \tag{4}$$

Notice that the contact pressure needs to be updated after every computational increment. When there is only wear, Eqn. (2) can be used to calculate the amount of wear in one cycle by setting $\Delta t = T_o$. Time advances NT_o by multiplying the wear in one cycle with N, giving the wear after N cycles. When wear and creep act together, Eqn. (4) should be used. In contrast to Eqn. (2), time advances by T_i ($T_i > T_o$) in Eqn. (4) and the accumulated wear during an effective cycle should not be used to multiple any cycle number for projection. Time advances by repeating Eqn. (4) one effective cycle after another.

Once the wear depth at the end of the effective cycle has been computed, the geometry is updated and the calculation repeated. However, it is important to appreciate that after updating the geometry, one cycle of a regular length needs to be computed to ensure that steady-state conditions have been met before proceeding with calculating the full effective cycle again.

2.2 Determining the period of the effective cycles

While the concept described above may appear to be obvious in retrospect, the challenge lies in establishing the criterion for calculating the length of T_i, and recognizing that it can change throughout a calculation. The length of the effective cycle T_i needs to be small enough to achieve a desired level of accuracy. The magnitude of T_i scales the wear in a proportional fashion. If T_i is too large, the development of the wear may cause excessive errors in the stress that is used for both the creep and wear calculations. Conversely, if T_i is too small, the computational efficiency is reduced. These constraints are valid even in the two limits where the

effects of creep are small and where the wear rate is small. In particular, wear during one cycle over a long period during which the contact pressure relaxes is not the same as wear during many cycles over which the same relaxation occurs.

Our approach is to use the change in contact pressure at any point along the interface as a measure of how the problem is affected by wear and creep during one effective cycle. It should be emphasized that we only need to focus on the change in contact pressure, since we use a Coulomb assumption that the local shear stress along a slipping contact, where wear is occurring, is proportional to the local contact pressure. We define a threshold for the maximum allowable change in contact pressure as $\varphi p_{m,i}$, where $p_{m,i}$ is the maximum contact pressure along the contact surface at the end of the i^{th} cycle. The parameter φ is chosen to balance accuracy and efficiency. One can run a simulation using a relatively large φ, say 10%, for a certain number of effective cycles, and then repeat the simulation using a smaller φ, say 5%. If the difference in contact pressure at the end of simulation for the two simulations is less than the numerical uncertainty of the model (and input parameters) or simulation requirement, then φ is considered to be sufficiently small. Otherwise one can reduce φ and continue with the testing. In this paper we give some indications of the appropriate choice for φ.

Figure 2 shows a flow chart of how the concept of an effective cycle is used in a numerical simulation. We start with an assumed period for the effective cycle, T_1, chosen to be small enough so that the maximum change of contact pressure at all points is expected to be much smaller than the threshold. After computing the maximum contact pressure and maximum change in contact pressure from this cycle, we then proceed with the next step in the calculation using an effective cycle set according to the relationship

$$T_{i+1} = \frac{\varphi p_{m,i}}{\Delta p_i} T_i \tag{5}$$

where T_{i+1} denotes the length of the next effective cycle to be used, T_i denotes the length of the current effective cycle, and Δp_i denotes the maximum change of contact pressure among all points at the contact surface during the i^{th} cycle. Note that the maximum change of contact pressure and the maximum contact pressure may be at different nodal points on the contact surface. Using this approach, we can dynamically predict and update the length of the next effective cycle based on the stress relaxation observed during the current cycle. In this way the change of contact pressure during each effective cycle will be close to, but not more than, the threshold.

3. Finite-element modeling

We have implemented the effective-cycle approach in ABAQUS to couple creep and fretting wear. In this section we will demonstrate a few examples. A Hertz contact under conditions of full slip will first be used to demonstrate the approach when creep and wear cause a global stress relaxation. A second set of calculations will show the effect of creep on wear in a problem where there is initially only partial slip in a Hertzian contact. The last set of calculations will illustrate the technique when there is a corner with a singular field and partial slip. In this last case, creep also has the effect of changing the singular field. In all these calculations, the morphological changes in the surface caused by wear were modeled by assigning eigenstrains to the surface elements, as described in an earlier work (Hu *et al.*, 2015), rather than by re-meshing. In all the calculations, the contacts were formulated using surface-to-surface contact pairs, with a kinematic constraint that the slave-surface nodes do not penetrate the master surface being enforced (Simulia, 2013). The frictional force was always modeled

using a Coulomb-friction law, with a constant coefficient of friction, μ. Both the indenter and the substrate are assumed to have identical material properties, but only the substrate wears.

A full set of the appropriate non-dimensional parameters for the different cases is presented in Table 2. In particular, it will be noted that we have chosen to normalize the wear coefficient, α_o, in terms of the Young's modulus, E, as $\alpha_o E$. The magnitude of the creep constant, A, is normalized by the modulus, power-law exponent, and period of vibration, as $AE^n T_o$.

3.1 Full slip with a Hertz contact

Figure 3 shows the geometry of Hertz contact between a cylindrical surface of radius R and a flat substrate. A fixed displacement, D_y, was applied to the top of the indenter in a direction normal to the interface so as to apply a pressure across the contact. An oscillating tangential displacement of fixed magnitude D_x was applied to the top surface, parallel to the interface. We used displacement-controlled boundary conditions, rather than force-controlled boundary conditions, to address the effects of stress relaxation. In the first set of calculations, the amplitude of the tangential displacement, D_x, was chosen to be large enough for the contact to experience full slip from the first cycle.

First we considered a scenario in which the initial wear and the initial creep make comparable contributions to stress relaxation at the interface. The case chosen corresponds to a ratio of the non-dimensional groups describing the effects of creep to wear of $AE^{n-1}T_o/\alpha_o = 1.1\times 10^{18}$, with $n = 4$ (Scenario 1 in Table 2). Figure 4 shows the contact pressure and wear profile at $t/T_o=1\times10^4$ (Figs. 4a and 4b) and $t/T_o=5\times10^4$ (Figs. 4c and 4d). It can be seen from Figs. 4a and 4c that although the initial effects of wear and creep on stress relaxation are comparable, the effects of creep decay with time compared with those of wear, since power-law creep is very

sensitive to the magnitude of the stresses, while wear has only a linear dependence on contact pressure. The effects of φ were much smaller than any numerical uncertainty below a value of $\varphi = 10\%$. φ could be increased to as much as about 30% before the discrepancy had a magnitude comparable to the numerical uncertainty. Little numerical efficiency is gained by increasing φ above 20%. Since one aspect of this study was to explore situations in which creep has a significant effect on the problem of wear, all of our wear calculations were repeated without creep, which was obtained by setting A to zero. In this particular case, the additional stress relaxation contributed to a reduced wear rate.

3.2 Partial slip with a Hertz contact

Even if a contact exhibits macroscopic stick, partial slip may occur around the edge of a contact edge, owing to local geometrical effects. For a Hertz contact, the partial slip region does not propagate owing to wear (Goryacheva *et al.*, 2001). However, we will show in this section that the effect of creep is to reduce the stress level, extend the region of partial slip across the interface, and turn the problem into one involving full slip.

In order to demonstrate the capability of an approach using effective cycles to model this scenario, we used the same parameters as in the previous two cases, but reduced the magnitude of the tangential displacement by a factor of two, so only the region of the interface around the circumference of the contact slipped initially (Scenario 2 in Table 2). The simulations were repeated with a range of φ up to 20%. Figures 5a and 5c show the evolution of contact pressures at $t/T_o = 1\times10^4$ and $t/T_o = 1\times10^5$, respectively, while Figs. 5b and 5d show the corresponding wear scars. In particular, one can note the non-slip region, corresponding to a region of no wear, at the center of the contact in Fig. 5b. At the start of simulation the slip region was limited to a

distance of $|x|/l > 0.18$ from the center. When φ is as high as 20% there is a slight effect on the wear scar beyond numerical error.

The effects of creep on the development of the wear scar can be seen very clearly in Fig. 5d. Without creep, the inner boundary of the wear scar remains at $|x|/l = 0.18$; it doesn't propagate towards the center, consistent with earlier observations (Goryacheva *et al.*, 2001). The relaxation associated with creep allows the slip region to propagate towards the center of the contact, eventually causing full slip along the interface. This results in much greater slip, and an enhanced wear rate, leading to a very different wear profile, which is particularly evident in Fig. 5d.

3.3 Contact with a sharp corner

In this last section, we consider a contact with a sharp corner, as shown in Fig. 6. The stress field is singular at a corner, providing an extreme example for modeling creep and wear. We chose a coefficient of friction equal to 0.35, so that partial slip occured near the corner under the initial conditions according to elasticity analysis (Churchman and Hills, 2006). In order to capture the behavior around the corner of interest, the mesh size was refined to $0.001l$. However, to ensure computational efficiency we only refined the corner on the left hand-side. We validated that the length of indenter was long enough so that the right corner of the contact had a negligible effect on the contact at the left corner, and that symmetrical meshing would have had a negligible effect on the stress distribution. As shown in Fig. 6, a fixed displacement D_y was applied at the top of the indenter, with an oscillating tangential displacement, D_x, parallel to the interface. The parameters used that corresponded to this case are listed as Scenario 3 in Table 2.

Figure 7 shows the contact pressure and wear depth. Figs. 7a and 7c show that the contact pressure field has a singularity of -0.380±0.008 at $t = 0$ near the corner. This confirms the accuracy of the numerical calculations, as it matches the theoretical value of -0.382 for the singularity with slip at a right-angled corner between two identical elastic materials and a friction coefficient of 0.35 (Churchman and Hills, 2006). In this case, this order of singularity is rapidly lost as a result of the creep, and drops to a steady-state value of -0.140±0.010. Although, we are unaware of published singularities for creeping materials with this particular contact geometry, this seems to be a reasonable value, and creep singularities have been calculated for bonded sharp notches with power-law creep (Zhu et al., 2011). Figures 7b and 7d show the wear scar at $t/T_o = 1\times10^4$ and $t/T_o = 1\times10^5$, respectively. Similar to Fig. 5, the stick-slip boundary does not move when there is no creep, and the wear depth is significantly underestimated. It should be noted that a value of $\varphi = 20\%$ approximately correspond to the condition when the discrepancy caused by the use of an effective cycle was comparable to numerical uncertainty.

3.4 Discussion

As shown in the previous sections, our effective cycle approach is robust in terms of the choice of φ. We further computed all three scenarios in the spirit of Archard's law, modeling the physical cycle explicitly, without using effective cycles. We compared the results of this explicit model with those from the effective cycle. Figure 8 shows the comparison. Owing to the high computational cost to calculate each physical cycle one by one, we let the system evolve for a shorter time in these calculations, since the goal was only to show that we lost no significant information by invoking effective cycles. Four effective cycles were invoked in the calculations, while this small number of effective cycles generated the same result of calculating many physical cycles.

For Scenario 1 in Fig. 8(a), the differences between the contact pressure and the wear depth using effective cycles with $\varphi = 10\%$ and without using effective cycles are less than 0.03% and 0.2%, respectively. We did similar validations for the other two scenarios in Fig. 8(b) and (c). These confirmed that the effective-cycle approach is reliable.

4. Conclusions

We have developed an effective cycle approach to couple the disparate time scales of creep, and vibration, which has enabled coupled creep and fretting-wear simulations. The length of the effective cycle is adjusted dynamically, on-the-fly, by limiting the change of contact pressure during each cycle to within a threshold consistent with both accuracy and efficiency. In real applications, a threshold that balances efficiency and accuracy can be determined by trials from large to small values until the contact pressure and wear depth curves converge.

In this study we investigated the effects of creep on wear for a range of scenarios. The relaxation of stress by creep has two effects. In problems involving full slip creep can have the effect of reducing the contact pressure, and hence the frictional work and wear damage. In problems involving partial slip, the reduction in contact pressure can cause the stick-slip boundary to move, leading to enhanced wear rates.

The method developed in this paper has been demonstrated to be robust in modeling various problems, where creep and wear cause global or localized stress redistribution. The approach automatically determines the appropriate time scale without the need of knowing which stress relaxation mechanism dominates. This approach may be useful to modeling various engineering problems where creep and wear interact and act simultaneously. For example, in a

peer project (Wang *et al.*, 2017), we have used this approach to couple creep and wear on the grid-to-rod interface in a pressurized water reactor.

Acknowledgements

This research was supported by the Consortium for Advanced Simulation of Light Water Reactors (http://www.casl.gov), an Energy Innovation Hub (http://www.energy.gov/hubs) for Modeling and Simulation of Nuclear Reactors under U.S. Department of Energy Contract No. DE-AC05-00OR22725.

References

Akhtar S. Khan, Huang, S., 1995. Continuum Theory of Plasticity. John Wiley & Sons, New York.

Archard, J.F., 1953. Contact and Rubbing of Flat Surfaces. Journal of Applied Physics 24, 981-988.

Bevill, S.L., Bevill, G.R., Penmetsa, J.R., Petrella, A.J., Rullkoetter, P.J., 2005. Finite element simulation of early creep and wear in total hip arthroplasty. Journal of Biomechanics 38, 2365-2374.

Churchman, C.M., Hills, D.A., 2006. General results for complete contacts subject to oscillatory shear. Journal of the Mechanics and Physics of Solids 54, 1186-1205.

Costa, H.L., Oliveira, M.M., de Mello, J.D.B., 2017. Effect of debris size on the reciprocating sliding wear of aluminium. Wear 376, 1399-1410.

Ding, J., Leen, S.B., McColl, I.R., 2004. The effect of slip regime on fretting wear-induced stress evolution. Int J Fatigue 26, 521-531.

Fouvry, S., Kapsa, P., Vincent, L., 2001. An elastic-plastic shakedown analysis of fretting wear. Wear 247, 41-54.

Frost, H.J., Ashby, M.F., 1982. Deformation Mechanism Maps: The Plasticity and Creep of Metals and Ceramics. Pergamon Press, Oxford, UK.

Gan, Z., Liu, H., Li, S., He, X., Yu, G., 2017a. Modeling of thermal behavior and mass transport in multi-layer laser additive manufacturing of Ni-based alloy on cast iron. International Journal of Heat and Mass Transfer 111, 709-722.

Gan, Z., Yu, G., He, X., Li, S., 2017b. Numerical simulation of thermal behavior and multicomponent mass transfer in direct laser deposition of Co-base alloy on steel. International Journal of Heat and Mass Transfer 104, 28-38.

Goryacheva, I.G., Rajeev, P.T., Farris, T.N., 2001. Wear in Partial Slip Contact. Journal of Tribology 123, 848-856.

Hegadekatte, V., Huber, N., Kraft, O., 2005. Finite element based simulation of dry sliding wear. Modelling and Simulation in Materials Science and Engineering 13, 57-75.

Hong, W., Cai, W., Wang, S., Tomovic, M.M., 2017. A Review for Mechanical Wear Debris Feature, Detection and Diagnosis. Chinese Journal of Aeronautics, in press.

Hu, Z., Lu, W., Thouless, M.D., Barber, J.R., 2015. Simulation of wear evolution using fictitious eigenstrains. Tribology International 82, Part A, 191-194.

Jacobs, O., Kazanci, M., Cohn, D., Marom, G., 2002. Creep and wear behaviour of ethylene–butene copolymers reinforced by ultra-high molecular weight polyethylene fibres. Wear 253, 618-625.

Johansson, L., 1994. Numerical-Simulation of Contact Pressure Evolution in Fretting. J Tribol-T Asme 116, 247-254.

Johnson, K., 1984. Contact mechanics. Cambridge University Press, Cambridge, UK.

Kasarekar, A.T., Bolander, N.W., Sadeghi, F., Tseregounis, S., 2007. Modeling of fretting wear evolution in rough circular contacts in partial slip. Int J Mech Sci 49, 690-703.

Kim, H.-K., Lee, Y.-H., Lee, K.-H., 2008. On the geometry of the fuel rod supports concerning a fretting wear failure. Nuclear Engineering and Design 238, 3321-3330.

Kim, K.-T., 2009. The study on grid-to-rod fretting wear models for PWR fuel. Nuclear Engineering and Design 239, 2820-2824.

Kim, K.-T., 2010a. The effect of fuel rod supporting conditions on fuel rod vibration characteristics and grid-to-rod fretting wear. Nuclear Engineering and Design 240, 1386-1391.

Kim, K.-T., 2010b. A study on the grid-to-rod fretting wear-induced fuel failure observed in the 16×16KOFA fuel. Nuclear Engineering and Design 240, 756-762.

Lai, G.Y., 1979. Factors affecting the performances of sprayed chromium carbide coatings for gas-cooled reactor heat exchangers. Thin Solid Films 64, 271-280.

Lee, K.-Y., Pienkowski, D., 1997. Reduction in the initial wear of ultrahigh molecular weight polyethylene after compressive creep deformation. Wear 203–204, 375-379.

Lu, W., Thouless, M.D., Hu, Z., Wang, H., Ghelichi, R., Wu, C.-H., Kamrin, K., Parks, D., 2016. CASL Structural Mechanics Modeling of Grid-to-Rod Fretting (GTRF). JOM 68, 2922-2929.

McColl, I.R., Ding, J., Leen, S.B., 2004. Finite element simulation and experimental validation of fretting wear. Wear 256, 1114-1127.

Mukras, S., Kim, N.H., Sawyer, W.G., Jackson, D.B., Bergquist, L.W., 2009. Numerical integration schemes and parallel computation for wear prediction using finite element method. Wear 266, 822-831.

Narasimhan, S.L., Larson, J.M., Whelan, E.P., 1981. Wear characterization of new nickel-base alloys for internal combustion engine valve seat applications. Wear 74, 213-227.

Oqvist, M., 2001. Numerical simulations of mild wear using updated geometry with different step size approaches. Wear 249, 6-11.

Põdra, P., Andersson, S., 1999. Simulating sliding wear with finite element method. Tribology International 32, 71-81.

Rezaei, A., Van Paepegem, W., De Baets, P., Ost, W., Degrieck, J., 2012. Adaptive finite element simulation of wear evolution in radial sliding bearings. Wear 296, 660-671.

Simulia, D., 2013. ABAQUS User's & Theory Manuals-Release 6.13, Providence, RI.

Takahashi, T., Nagayoshi, T., Kumano, M., Sasaki, K., 2002. Thermal Plastic-elastic Creep Analysis of Engine Cylinder Head. SAE International.

Teeter, M.G., Parikh, A., Taylor, M., Sprague, J., Naudie, D.D., 2015. Wear and Creep Behavior of Total Knee Implants Undergoing Wear Testing. The Journal of Arthroplasty 30, 130-134.

Wang, H., Hu, Z., Lu, W., Thouless, M.D., 2013. A mechanism-based framework for the numerical analysis of creep in zircaloy-4. Journal of Nuclear Materials 433, 188-198.

Wang, H., Hu, Z., Lu, W., Thouless, M.D., 2017. The effect of coupled wear and creep during grid-to-rod fretting. Nuclear Engineering and Design 318, 163-173.

Williams, J.A., 2005. Wear and wear particles - some fundamentals. Tribology International 38, 863-870.

Zhu, H., Xu, J., Feng, M., 2011. Singular fields near a sharp V-notch for power law creep material. International Journal of Fracture 168, 159-166.

Figures

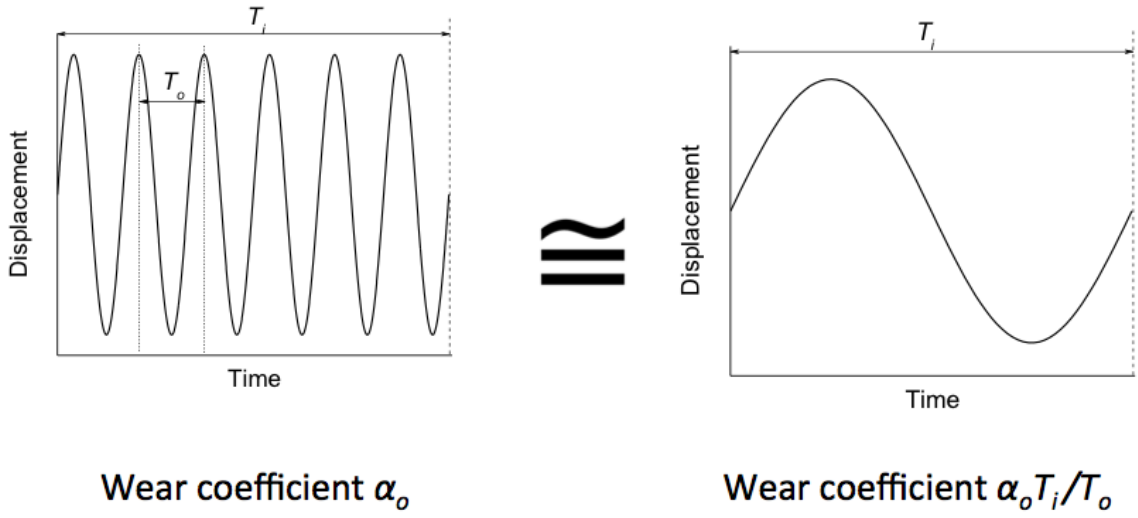

Figure 1: The concept of an effective cycle with a period T_i that uses a magnified wear coefficient to represent many physical vibration cycles. Wear and creep calculations are fully coupled using the effective cycle. In the finite-element calculations the period T_i is discretized into several time steps to calculate the evolution of the stress and displacement fields. The effective-cycle approach greatly accelerates the calculation since T_i/T_o is a large number. The length of the effective cycle is adjusted dynamically, on-the-fly, by limiting the change of contact pressure during each cycle to within a threshold consistent with both accuracy and efficiency.

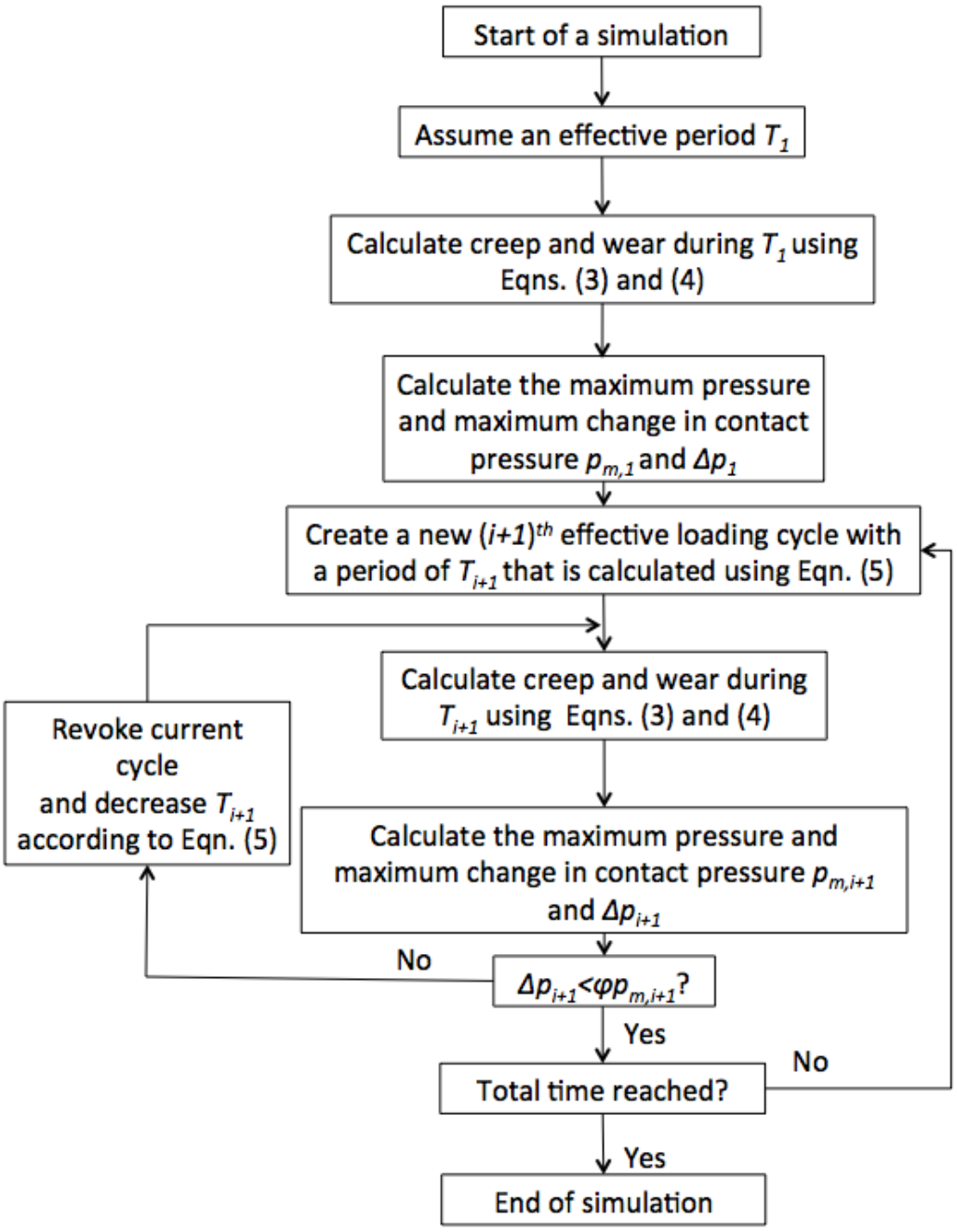

Figure 2: Flow chart to illustrate the process for the coupled wear and creep calculation.

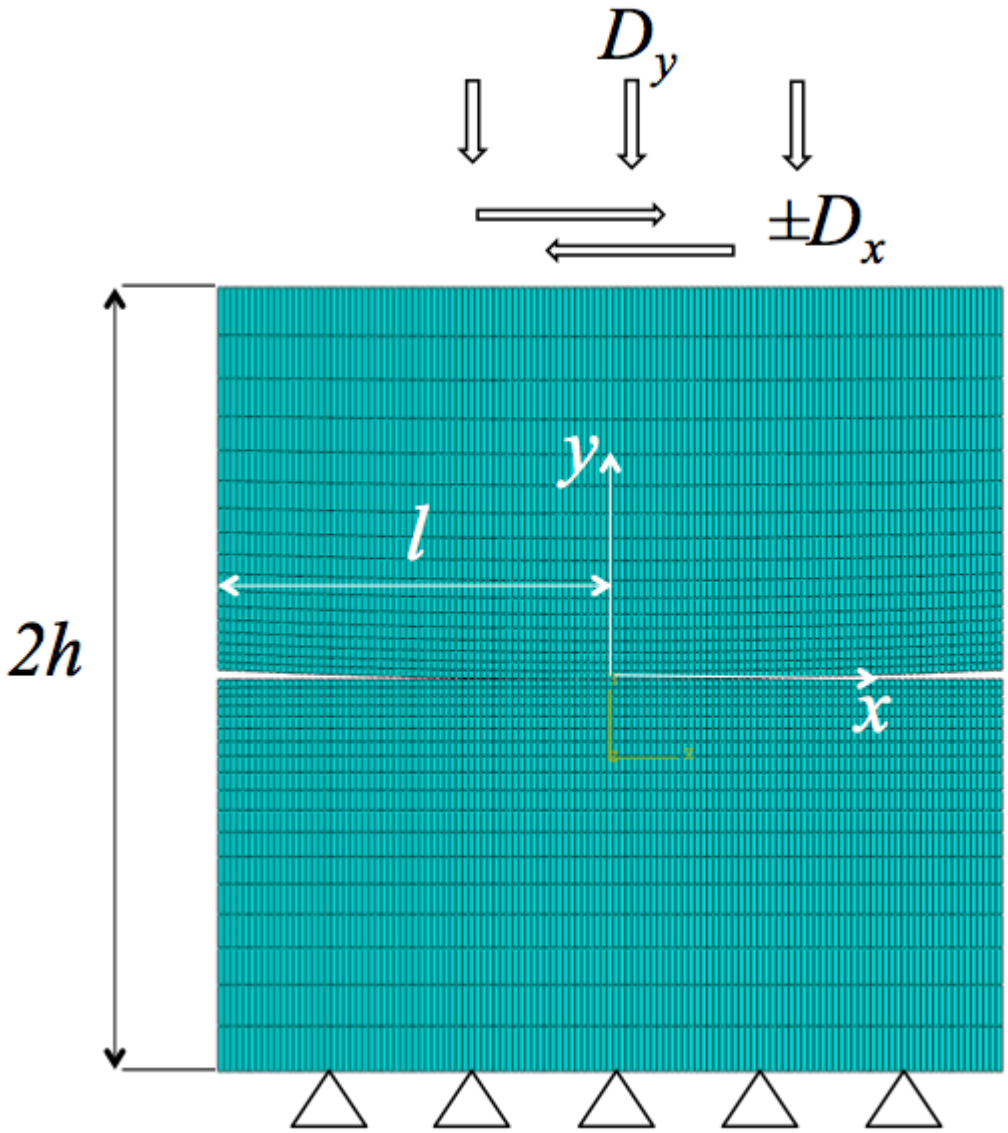

Figure 3: A Hertz contact between a cylindrical surface of radius R (top) and a flat substrate. A fixed normal displacement of magnitude D_y applied to the top surface, along with an oscillating tangential displacement of magnitude D_x.

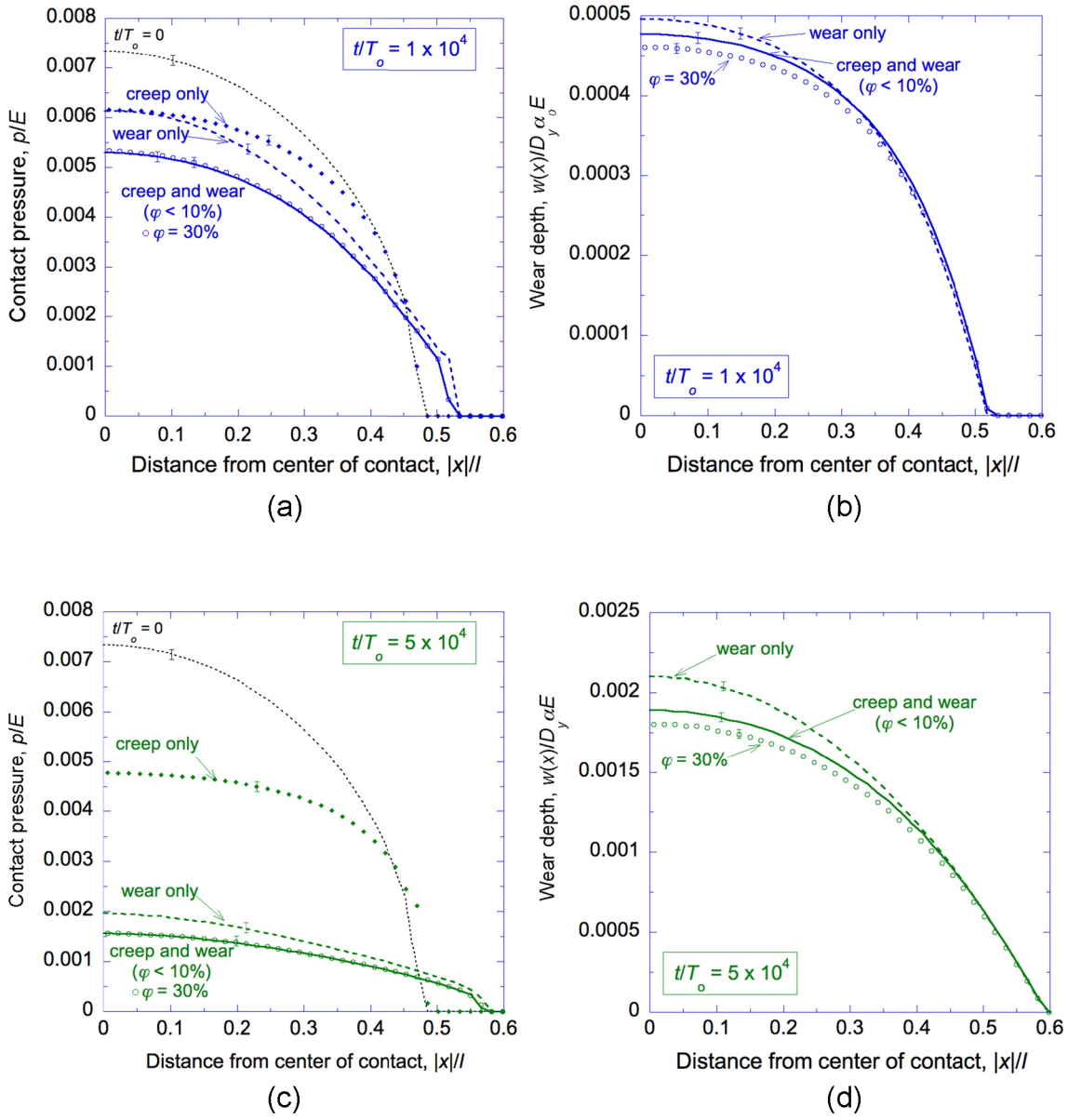

Figure 4: The conditions of Scenario 1 in Table 2 correspond to a case where creep and wear initially have comparable effects on stress relaxation. The resultant stress distributions are shown for **(a)** $t/T_o=1\times10^4$ and **(c)** $t/T_o=5\times10^4$. The contact pressures that evolve when only creep or wear occurs are shown for reference, which were obtained by switching off the wear or creep calculation. The wear depths that evolve are shown for **(b)** $t/T_o=1\times10^4$ and **(d)** $t/T_o=5\times10^4$, with the effects of wear only being shown for reference. The contact pressure is relatively insensitive to the choice of φ. The wear depth is slightly more sensitive, with effects larger than the numerical uncertainty being observed for $\varphi > 10\%$. However, even for $\varphi = 30\%$, the effects are relatively minor.

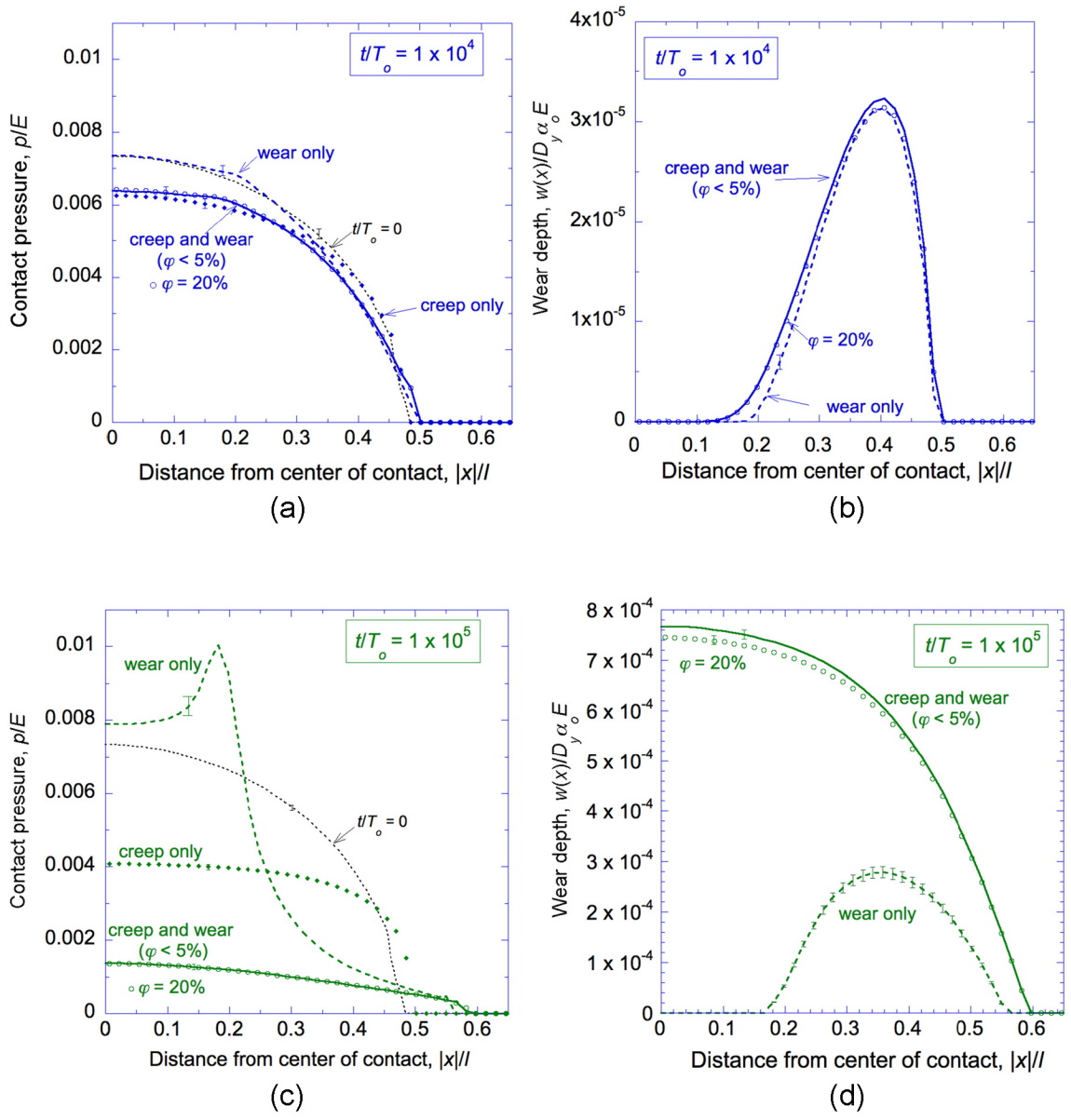

Figure 5: Contact pressure and profile of the wear depth for a partial-slip Hertz contact at $t/T_o=1\times10^4$ for **(a)** and **(c)**, and $t/T_o=1\times10^5$ for **(b)** and **(d)**, using the conditions of Scenario 2 in Table 2. The stress relaxations for creep only and wear only are shown for reference, which were obtained by switching off the wear or creep calculation. Without creep, the inner boundary of the wear scar remains at $|x|/l$ = 0.18; it doesn't propagate towards the center. The relaxation associated with creep allows the slip region to propagate towards the center of the contact, eventually causing full slip along the interface.

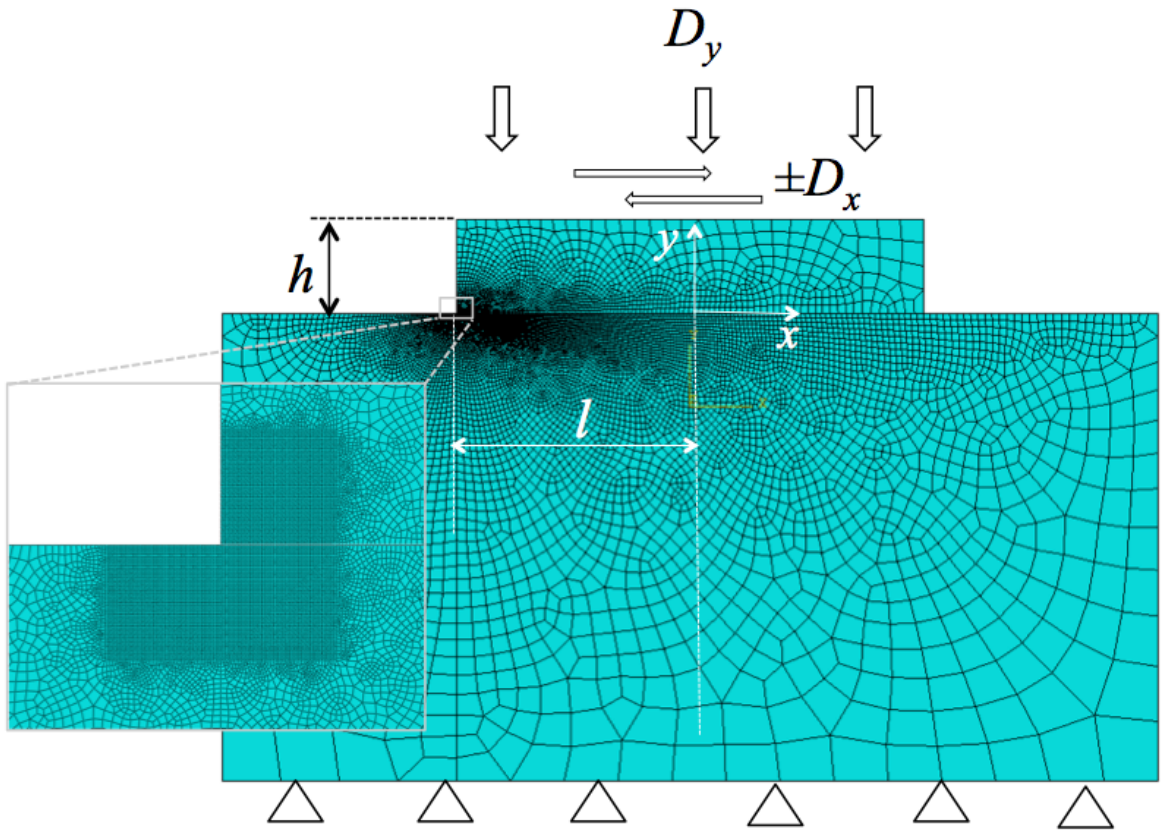

Figure 6: A complete contact with sharp corners under a fixed normal displacement D_y applied to the top, along with an oscillating tangential displacement of magnitude D_x.

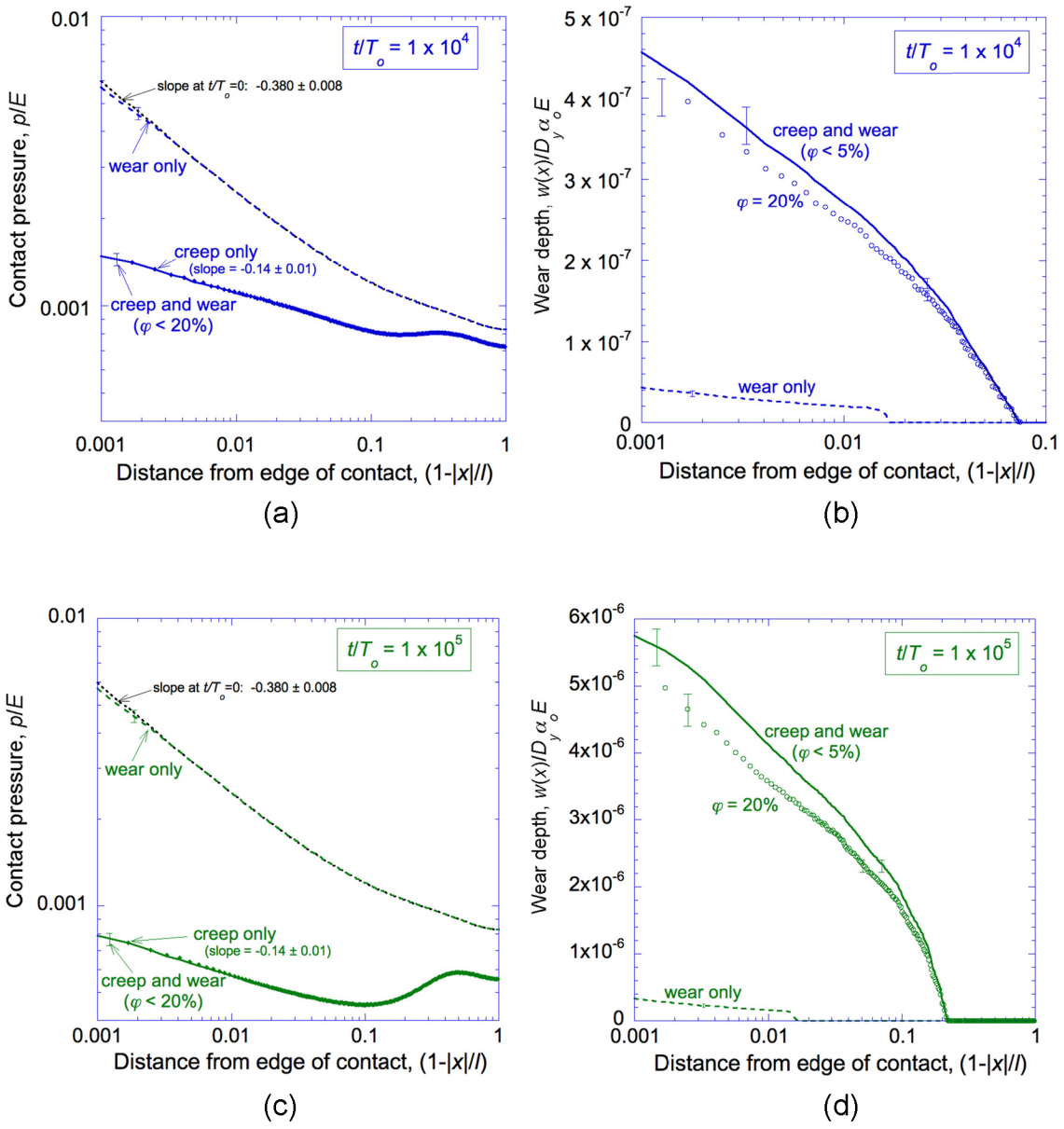

Figure 7: Contact pressure and profile of the wear depth for a complete contact with sharp corners that experiences partial slip, using the conditions of Scenario 3 in Table 2. Shown are at time $t/T_o=1\times10^4$ for **(a)** and **(c)**, and $t/T_o=1\times10^5$ for **(b)** and **(d)**. Creep dominates the stress evolution. The singularity of the contact pressure at $t/T_o=0$ matches the theoretical value of -0.382 and drops due to creep. The stick-slip boundary does not move when there is no creep, and the wear depth is significantly underestimated.

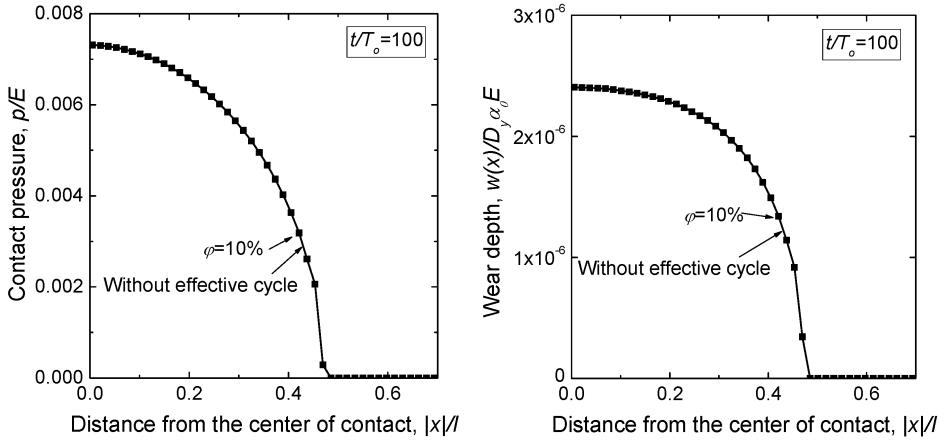
0.008
0.006
0.004
0.002
0.000
Contact pressure, p/E
t/T_o=100
φ=10%
Without effective cycle
0.0
0.2
0.4
0.6
Distance from the center of contact, |x|/l
3x10^-6
2x10^-6
1x10^-6
0
Wear depth, w(x)/D_y0αE
t/T_o=100
φ=10%
Without effective cycle
0.0
0.2
0.4
0.6
Distance from the center of contact, |x|/l

(a)

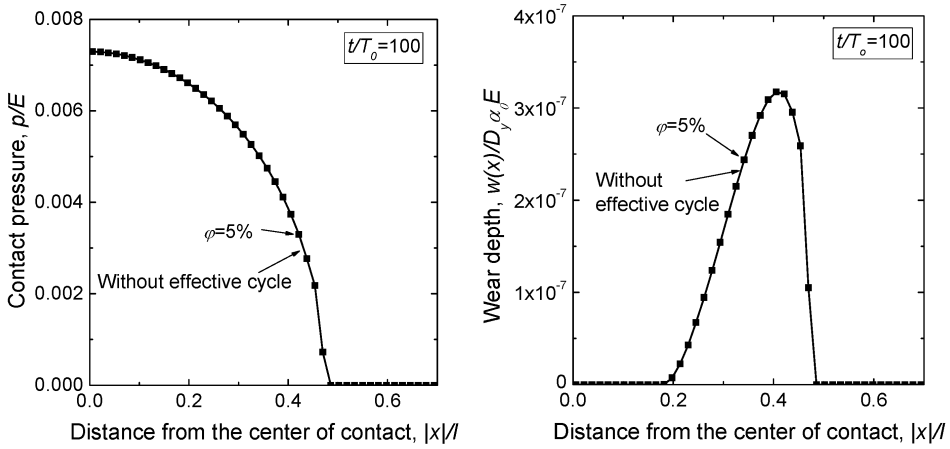
0.008
0.006
0.004
0.002
0.000
Contact pressure, p/E
t/T_0=100
φ=5%
Without effective cycle
0.0
0.2
0.4
0.6
Distance from the center of contact, |x|/l
4x10^-7
3x10^-7
2x10^-7
1x10^-7
0
Wear depth, w(x)/D_y0αE
t/T_o=100
φ=5%
Without
effective cycle
0.0
0.2
0.4
0.6
Distance from the center of contact, |x|/l

(b)

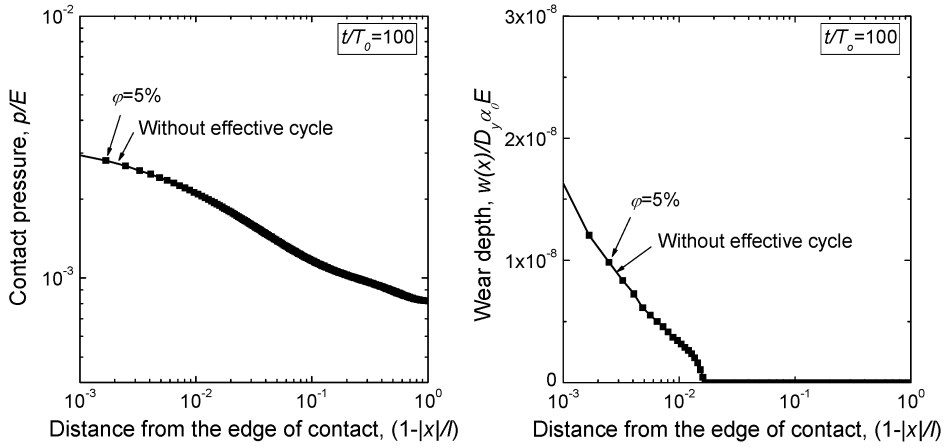
10^-2
10^-3
Contact pressure, p/E
t/T_0=100
φ=5%
Without effective cycle
10^-3
10^-2
10^-1
10^0
Distance from the edge of contact, (1-|x|/l)
3x10^-8
2x10^-8
1x10^-8
0
Wear depth, w(x)/D_y0αE
t/T_o=100
φ=5%
Without effective cycle
10^-3
10^-2
10^-1
10^0
Distance from the edge of contact, (1-|x|/l)

(c)

Figure 8: Comparison of results using effective cycles (dots) and without using effective cycles (line) for the conditions of **(a)** Scenario 1, **(b)** Scenario 2, and **(c)** Scenario 3 in Table 2. Four effective cycles were invoked in the calculations, while this small number of effective cycles generated the same result of calculating many physical cycles.

Tables

Table 1: Nomenclature

l	Semi length of the indenter
h	Height of the indenter
D_x	Tangential displacement
D_y	Normal displacement
R	Radius of the indenter in the Hertz contact
E	Young's modulus
v	Poisson's ratio
α_o	Wear coefficient
w_i	Wear depth increment during the i^{th} cycle
w	Wear depth
p	Contact pressure
μ	Friction coefficient
Δ	Slip distance
σ_{VM}	Von Mises effective stress
ε_{VM}	Von Mises effective creep strain
A	Creep coefficient
n	Creep power order
t	Time
T_o	Period of vibration
T_i	Period of the i^{th} effective cycle
φ	Percentage threshold of allowable contact pressure change during one effective cycle
Δp_i	Maximum change of contact pressure among all points at the contact surface during the i^{th} cycle
$p_{m,i}$	Maximum contact pressure along the contact surface at the end of the i^{th} cycle or at the beginning of the next $(i+1)^{th}$ cycle

Table 2: Dimensionless parameters

	Scenario 1 (Hertz full slip)	Scenario 2 (Hertz partial slip)	Scenario 3 (Complete full slip)
D_x/l	8×10^{-3}	4×10^{-3}	2×10^{-5}
D_y/l	0.01	0.01	0.004
R/l	20	20	NA
l/h	1	1	1
μ	0.2	0.2	0.35
v	0.25	0.25	0.25
n	4	4	4
AE^nT_o	4×10^{15}	4×10^{15}	4×10^{12}
α_oE	3.5×10^{-3}	7×10^{-3}	7×10^{-3}